Journal Name

ARTICLE

Cocrystals of Spironolactone and Griseofulvin Based on an *in Silico* Screening Method

Received 00th January 20xx,
Accepted 00th January 20xx

DOI: 10.1039/x0xx00000x

www.rsc.org/

Tudor Grecu,[a] Rafel Prohens,[b c] James F. McCabe,[a] Elliot J. Carrington,[d] James S. Wright,[d] Lee Brammer,[d] and Christopher A. Hunter*[e]

Cocrystal formation is considered as one of the most effective solid-state methods to alter the physicochemical properties of active pharmaceutical ingredients (APIs). *In silico* methods for cocrystal prediction are mostly based on structural and energetic considerations. We have developed a computational method that ranks the probability of cocrystal formation of APIs with large databases of crystal coformers (CCFs). This approach is based on using molecular electrostatic potential surfaces to assess molecular complementarity between two cocrystal components. The screening tool was applied to two low solubility drugs, namely griseofulvin and spironolactone. Promising coformer candidates were selected from a database of 310 pharmaceutically acceptable CCFs, and experimental screening was carried out. Novel solid forms were obtained by liquid-assisted grinding and were characterised by XRPD, DSC, TGA and IR. One new cocrystal of griseofulvin and two new cocrystals of spironolactone were identified, and the crystal structures were determined from the XRPD patterns. For these systems, phenols tend to act as successful H-bond donors in forming cocrystals, while carboxylic acids only give rise to physical mixtures of the two components.

Introduction

The exploration of active pharmaceutical ingredient (API) solid state chemistry is an integral part of drug discovery and pharmaceutical development.[1] Solubility properties and the dissolution rate of a solid drug are key parameters in dictating oral bioavailability.[2] With the use of high-throughput screening methodology and combinatorial chemistry, the number of poorly soluble APIs has risen dramatically.[3] Drugs exhibiting poor bioavailability are categorised as Biopharmaceutical Classification System (BCS) class II and class IV, based on their low solubility properties.[4] Several approaches in drug formulation have been designed to improve drug solubilisation in the gastrointestinal tract. Non-covalent approaches include the use of cyclodextrin inclusion compounds,[5] solid dispersions,[6] amorphous forms[7] as well as salt[8] and cocrystal formation.[9]

Pharmaceutical cocrystals are molecular adducts of definite stoichiometry where one component is a neutral API and the other is a neutral pharmaceutically acceptable crystal coformer (CCF) and both components are solids at room temperature.[10] The CCFs are usually selected from the GRAS (Generally Regarded as Safe)[11] and EAFUS (Everything Added to Food in the United States)[12] lists if the resulting cocrystals are to be considered suitable for drug development. The benefit of cocrystallisation is that non-ionisable API molecules can also be targeted, so the list of potential CCFs is more comprehensive than for salt formation. In recent years, the exploration of pharmaceutical cocrystals has led to the successful enhancement of physicochemical properties of APIs, such as thermal, humidity and thermodynamic stability.[13] Other important pharmaceutical properties that have been improved through cocrystal formation are clinical performance and manufacturability.[14]

In 2013, the FDA considered cocrystals as 'API-excipient' complexes that were treated as drug product intermediates.[15] The new 2016 FDA draft guidance explains that cocrystals should be classified as special cases of solvates, where the second component is non-volatile.[16] From a regulatory perspective, a cocrystal will be treated in the same way as a new polymorph of the same API and not as a different chemical entity, as is the case for salts. The new classification has consequences for the development of cocrystals in the pharmaceutical industry due to the simplification of the

[a] *AstraZeneca, Silk Road Business Park, Macclesfield, Cheshire SK10 2NA, UK.*
[b] *Unitat de Polimorfisme i Calorimetria, Centres Científics i Tecnològics, Universitat de Barcelona, Baldiri Reixac 10, 08028 Barcelona, Spain.*
[c] *CIRCE Crystal Engineering, Isaac Newton, s/n. ParcBit, 07121 Palma de Mallorca, Spain.*
[d] *Department of Chemistry, University of Sheffield, Sheffield S3 7HF, UK.*
[e] *Department of Chemistry, University of Cambridge, Lensfield Road, Cambridge CB2 1EW, UK. Email: herchelsmith.orgchem@ch.cam.ac.uk.*
Electronic supplementary information (ESI) available: List of all 310 CCFs virtually screened, powder XRD profiles with Rietveld fits and IR spectra. See DOI: 10.1039/x0xx00000x

multicomponent complex regulatory landscape. For example, it will be possible to use existing regulatory documents to establish potency, purity and stability of a cocrystal API.[17]

The process of cocrystal screening can generally be broken down into sample preparation, characterisation and determination of properties.[18] Conventional experimental cocrystal screens employed are solution based, such as slow evaporation, cooling and vapour diffusion.[19] These methods are useful as they can yield suitable crystals for structure determination by single crystal X-ray diffraction. However, single crystal growth is inherently slow and there is a high risk of hydrates and solvates being formed.[20] Furthermore if the solubilities of the API and CCF are very different, precipitation of the least soluble component is more likely to take place rather than the desired cocrystal.[21] Neat grinding (NG) and liquid-assisted grinding (LAG) experiments were shown to be more efficient at identifying cocrystals as they avoid solvent competition that can lead to precipitation of individual components.[22] Moreover, advances in powder X-ray diffraction methods mean that crystal structure solutions can be obtained from powder data with good accuracy.[23]

In this work, we apply a virtual cocrystal screening method[24] to two BCS class II APIs, griseofulvin (GSF) and spironolactone (SPN).[25-27] The *in silico* screening method has been previously validated using experimental cocrystal data reported in the literature[28] and was successfully applied to obtain seven novel cocrystals of nalidixic acid.[29] This methodology is not limited to cocrystal prediction. It can be applied to formation of ionizable multi-component adducts such as salts and propensity to form solvates for a specific API. The computational approach uses calculated molecular electrostatic potential surfaces (MEPS) to identify surface site interaction points (SSIPs).[24] The SSIPs can be used to assess the molecular recognition properties of the entire surface of the molecule,[30] and here, they are used to calculate the solid state interaction site pairing energy, E, defined in Equation 1, which is the sum of all intermolecular interactions in a solid. The SSIPs of a molecule are each described by an interaction parameter, ε_i, which is positive for a H-bond donor site (or positive region on the MEPS) and negative for a H-bond acceptor site (or negative region on the MEPS). The energy of interaction between two SSIPs, i and j, is given by the product $\varepsilon_i\varepsilon_j$. The stability of a solid is estimated by a hierarchical pairing of charge-complementary SSIPs to obtain E: the most positive SSIP pairs the most negative SSIP, followed by sequential association of the second most positive and negative SSIPs until no more pairwise interactions can be formed.[31]

$$E = \sum_{ij} \varepsilon_i \varepsilon_j \qquad \text{Eq. 1}$$

The difference in the pairing energy between the pure components and the cocrystal (ΔE) provides a measure of the probability of forming a cocrystal (eq. 2):

$$\Delta E = -(E_{cc} - E_1 - E_2) \qquad \text{Eq. 2}$$

where E_{cc}, E_1 and E_2 are the interaction site pairing energies of the cocrystal and the pure solids, 1 and 2, respectively.

Validation of the ΔE parameter was recently provided by a CCF exchange experiment using caffeine cocrystals.[32] The experiment involved grinding multiple CCFs with caffeine and using the identities of the cocrystals that formed in the mixtures to establish a cocrystal stability ranking. The experimental stability ranking for the caffeine cocrystals matched the previously published ranking of ΔE values.[24]

GSF is an antifungal BCS class II drug that has been reported to exhibit antiviral and anticancer effects in mammalian systems.[33] An enhancement in GSF bioavailability was obtained by nanoparticle preparation from water-dilutable microemulsions,[34] the use of drug-polymer solid solutions[35] and nanocapsules.[36] In a cocrystal screen, grinding of GSF with 40 coformers only yielded a 2:1 GSF-acesulfame cocrystal hydrate, where the two cocrystal components interact via the water molecule.[25] The screen also yielded GSF solvates with acetonitrile, nitromethane and nitroethane.[37] More recently, a drug-polymer cocrystal was reported between GSF and polyethylene glycol.[38]

SPN has been extensively used as a potassium-sparing diuretic. It is a non-ionisable BCS class II drug that acts as a steroidal aldosterone antagonist.[39] Improvement in SPN biovailability was obtained by nanosuspension formulation,[40] drug micronization and the use of β-cyclodextrins.[41] In the literature, there are also two studies concerned with the cocrystallisation of SPN. A 1:1 SPN-saccharin cocrystal hemihydrate has been reported, where crystal packing remained largely unchanged after dehydration.[26] In a cocktail grinding study, several CCFs were ground simultaneously with SPN,[27] and novel powder patterns were obtained with benzoic, salicylic and gentisic acid.

Here we describe the structures of new cocrystals of both GSF and SPN that were obtained after *in silico* screening of a database of 310 pharmaceutically acceptable CCFs.

Experimental

Virtual cocrystal screen: Molecular structures of GSF, SPN and all 310 CCFs were drawn in an extended conformation using the TorchLite software,[42] so that the functional groups were exposed and available for interaction. The structures were energy minimised using the XED3 force field implemented in TorchLite, and the MEPS were calculated using DFT (B3LYP 6-31G*) in Gaussian 09.[43] The MEPS were then converted into a set of SSIPs using the method described previously.[27b] The increase in stability of the 1:1 cocrystal compared to the two pure components was estimated for all CCF-GSF and CCF-SPN combinations based on the difference in the interaction site pairing energies, ΔE, calculated using Equations 1 and 2 above.

Materials: GSF, SPN, all selected CCFs and solvents were purchased from Sigma-Aldrich and used as received.

Grinding: Grinding experiments were performed by mixing stoichiometric amounts of GSF and SPN (20 mg) with CCFs in a 5 mL stainless steel grinding jar containing a grinding ball 7 mm in diameter. In LAG experiments, 15 µl of acetonitrile or *n*-heptane was also added. Neat grinding was carried out for some systems where the coformers were highly soluble or had

low melting points: phenol, 4-*tert*-butylphenol, 2-phenyl phenol, indole, skatole and xylenols. The mixtures were ground on a Retsch MM 200 mixer mill for 20 to 45 minutes at 30 Hz.

X-ray Powder Diffraction (XRPD) Measurements: Powder samples were mounted on a silicon wafer mount and analyzed on a PANalytical CubiX PRO diffractometer with a copper long-fine focus tube running at 45 kV and 40 mA (λ = 1.5418 Å). Samples were measured in reflection geometry in the θ–2θ configuration over a scan range from 2° to 40° 2θ with 1.9 s exposure per 0.0025° increment.

Infrared Spectroscopy (IR): IR spectra were recorded with a universal ATR sampling accessory on a Perkin-Elmer Spectrum 100 Fourier transform spectrophotometer over a range from 400 to 4000 cm^{-1} with a resolution of 1 cm^{-1} (eight scans). The spectra were processed with the Spectrum v 10.03.07 software.

Differential Scanning Calorimetry (DSC): DSC measurements were performed using a Discovery DSC calorimeter. About 3 mg of solid material was weighed into a T_0 aluminium pan that was sealed hermetically with an aluminium lid. Samples were equilibrated at 25°C and then heated to 225°C or 235°C at a rate of 10°C min^{-1}.

Thermogravimetric analysis (TGA): TGA measurements were performed on a TA Q5000 instrument. An open alumina crucible was used to heat the sample from 25°C to the required temperature at a rate of 10°C/min under a nitrogen stream.

XRPD structure determination: For the GSF-4-*tert*-butylphenol cocrystal, a Panalytical X'Pert PRO MPD instrument with capillary configuration in transmission geometry, focusing elliptic mirror and PIXcel detector working at a maximum detector active length of 3.347º 2θ, was used. $Cu_{K\alpha}$ radiation (λ = 1.5418 Å) was selected with focalizing 0.01 and 0.02 radians Soller slits. The instrument was operated at 45 kV and 40 mA. Samples were placed in Lindemann capillaries of diameter 0.7 mm and were measured from 2° to 70° 2θ, with a step size of 0.013° and a data collection time of 16 hrs. The powder pattern was indexed to a monoclinic cell of approximate volume 1302 $Å^3$ by means of Dicvol04[44] and the space group was determined to be $P2_1$ from the systematic absences. Based on the calculated density, it was established that there was one independent molecule of GSF and one independent molecule of 4-*tert*-butylphenol in the asymmetric unit. The crystal structure was determined by direct space methodologies starting from a molecular model optimized with the commercial software SPARTAN by means of the program FOX[45] with the parallel tempering algorithm. Constraints on molecular geometry were applied, in particular considering aromatic rings as rigid groups. Several trials of 20 million runs were performed. Refinement of the structure was performed by the Rietveld method[50] using FullProf[46] and converged to χ^2 = 6.212. Figure S1 of the supplementary information depicts the final Rietveld plot.

For the SPN-phenol and SPN-2,5-xylenol cocrystals, solid samples were loaded into a 0.7 mm borosilicate capillary. X-ray diffraction data were collected (λ = 0.82665 Å) at beamline I11 at Diamond Light Source,[47] using a wide angle (90°) PSD detector comprising multiple Mythen-2 modules. Five pairs of five-second scans were conducted at room temperature, related by a 0.25° detector offset to account for gaps between detector modules, in addition to two pairs of one-second scans before and afterwards, to check for beam damage to the sample. All resulting patterns were summed to give the final pattern for structural analysis. Both powder patterns were indexed to a single phase using the TOPAS program.[48] The new unit cells were then fitted using single-phase Pawley refinements.[49] SPN-phenol crystallised in an orthorhombic unit cell and SPN-2,5-xylenol in a monoclinic unit cell. These were compared with existing crystal structures for SPN and the corresponding CCF in the CCDC, already established from single-crystal X-ray diffraction. No match with any single phase or mixture of the two phases was found. The starting model used for the Rietveld refinement,[50] conducted using TOPAS, was rigid-body models (represented as z-matrices) of the two cocrystal pure components from the single-crystal structures. These rigid bodies were allowed to translate and rotate over 10000 iterations to find the correct minimum. The model for the SPN-phenol cocrystal structure was refined using the Rietveld and converged to χ^2 = 7.210. For the SPN-2,5-xylenol cocrystal, the Rietveld refinement converged χ^2 = 6.115. Figure S2 and S3 of the supplementary information depict the final Rietveld plots for the SPN-phenol and SPN-2,5-xylenol cocrystals respectively.

Results and Discussion

A database of 310 CCFs was used to calculate a hierarchical list based on the stability of the potential GSF and SPN cocrystals compared to the sum of the two pure components (ΔE expressed in kJ mol^{-1}). For a list of all the 310 CCFs used, please see the Supporting Information. Table 1 shows the top 35 CCFs that are predicted most likely to yield cocrystals with GSF and SPN along with their corresponding ΔE values. Both GSF and SPN are predicted to form favourable interactions with good H-bond donors such as carboxylic acids and phenols, because they have carbonyl groups that can act as H-bond acceptors and no H-bond donors. GSF was subjected to experimental screening with the CCFs from the left side of Table 1 while SPN was tested with the right-hand side CCFs. Just over 10% of the CCF database with ΔE values greater than 10 kJ mol^{-1} was therefore screened for each API.

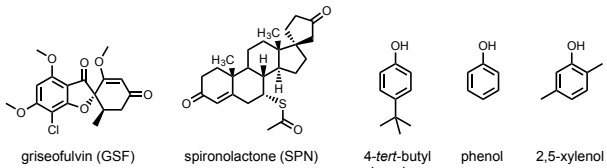

Figure 1. Chemical structures of GSF, SPN and the CCFs that formed cocrystals as judged by XRPD.

Table 1. Top ranked CCFs based on Δ*E*.

Griseofulvin (GSF)		Spironolactone (SPN)	
CCF	Δ*E* / kJ mol^{-1}	CCF	Δ*E* / kJ mol^{-1}
3,4-dihydroxybenzoic acid	28.3	3,4-dihydroxybenzoic acid	26.8
Etidronic acid	27.2	Resorcinol	25.8
Resorcinol	26.2	Etidronic acid	24.6
Citric acid	22.8	Sucralose	22.0
Tartaric acid	22.5	Tartaric acid	20.1
Camphoric acid	22.2	Citric acid	19.5
Malonic acid	21.7	Propyl gallate	18.4
Propyl gallate	20.6	*Tert*-butylhydroquinone	17.7
Sucralose	20.2	Malic acid	17.1
Malic acid	20.0	Oxalic acid	16.6
Oxalic acid	19.3	3-hydroxybenzoic acid	16.3
Tert-butylhydroquinone	18.9	4-hydroxybenzoic acid	16.2
2,5-dihydroxybenzoic acid	18.4	Fumaric acid	16.1
3-hydroxybenzoic acid	17.8	2,5-dihydroxybenzoic acid	15.5
4-hydroxybenzoic acid	17.7	L-rhamnose	15.0
L-rhamnose	16.7	Sucrose	14.6
Succinic acid	15.7	Maltose	14.3
Thiodipropionic acid	15.4	L-tyrosine	13.8
Ascorbic acid	14.7	Succinic acid	12.8
L-tyrosine	14.6	Thymol	12.7
Sucrose	14.5	Thiodipropionic acid	12.6
Maltose	14.2	2-phenyl phenol	12.5
L-glutamic acid	14.0	Ascorbic acid	12.5
Adipic acid	13.5	Urea	12.5
Folic acid	12.8	2,4-dihydroxybenzoic acid	12.5
Taurine	12.2	L-glutamic acid	12.4
1-hydroxy-2-naphthoic acid	11.8	Butylated hydroxytoluene	11.8
2,5-xylenol	11.4	1-hydroxy-2-naphthoic acid	11.5
2-phenyl phenol	11.4	2,5-xylenol	11.4
4-*tert*-butylphenol	11.1	Taurine	11.3
Pyridoxine	11.1	Adipic acid	11.3
Skatole	10.7	4-*tert*-butylphenol	11.0
D-isoascorbic acid	10.6	3,4-xylenol	10.4
Phenol	10.5	Phenol	10.1
D-ribose	10.5	Folic acid	9.8

Table 2. Crystallographic data for griseofulvin and spironolactone cocrystals.

	GSF – 4-tert-butylphenol	**SPN-phenol**	**SPN-2,5-xylenol**
Stoichiometry	1:1	1:1	1:1
crystal system	Monoclinic	Orthorhombic	Monoclinic
space group	$P2_1$	$P2_12_12_1$	$P2_1$
a (Å)	13.10068 (14)	18.5914(4)	24.7971(6)
b (Å)	8.65708 (10)	22.6434(5)	10.2080(3)
c (Å)	11.62420 (15)	6.4703(2)	6.3069(1)
α (°)	90	90	90
β (°)	98.9448 (8)	90	112.538(2)
γ (°)	90	90	90
Z	2	2	2
V (Å^3)	1302.31	2723.8(1)	1474.52(6)
Indices of fit	$\chi^2 = 6.212$	$\chi^2 = 7.210$	$\chi^2 = 6.115$
CCDC	1517121	1517122	1517123

Experimental cocrystal screen

Liquid-assisted grinding (LAG) was the experimental method of choice due to efficiency and speed. The chemical structures of the two APIs and the CCFs that led to successful cocrystallisation by this method are shown in Figure 1.

Griseofulvin

Cocrystal formation was initially studied by LAG of 1:1 stoichiometric ratios of GSF with the corresponding CCFs using *n*-heptane as a catalytic solvent. This solvent does not readily form solvates with small organic molecules and minimises sample dissolution due to the low polarity. The LAG mixtures were analysed by XRPD to identify the form and crystallinity of the samples. A system was defined as a hit if, following grinding, it displayed a different powder pattern compared to the patterns of the two pure components. Analysis of the XRPD patterns revealed that physical mixtures of the components or peaks corresponding to pure GSF were obtained in most cases (data not shown). The grinding of a 1:1 GSF and 4-*tert*-butylphenol mixture for 45 minutes at 30 Hz gave a powder pattern different from the pure components but the crystallinity of the sample was poor. Acetonitrile was tried as an alternative LAG solvent under the same grinding conditions and a highly crystalline phase was obtained (Figure 2a, green trace).

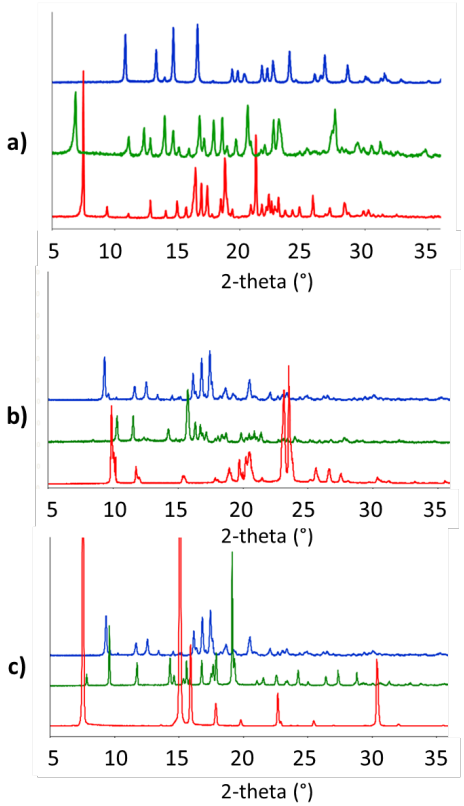

Figure 2. XRPD patterns of (a) griseofulvin (blue), 4-*tert* butylphenol (red) and a 1:1 mixture after LAG (green); (b) spironolactone (blue), phenol (red) and a 1:1 mixture after LAG (green); (c) spironolactone (blue), 2,5-xylenol (red) and a 1:1 mixture after LAG (green).

Furthermore, the reflections arising from the starting materials were absent, suggesting that a new pure phase has been obtained. The new XRPD pattern was compared to the calculated XRPD pattern of a GSF-acetonitrile solvate that has been previously discovered (CCDC refcode PINMOQ) [35]. The powder pattern obtained from the crystal structure of the GSF-acetonitrile solvate was completely different from that of the one obtained following the LAG mixture of GSF and 4-*tert*-butylphenol.

The thermal stability of this sample was also analysed by DSC (Figure 3a). The endothermic peaks that do not correspond to the melting points of the pure components suggest a cocrystal. The thermogram shows a single sharp endotherm with melting onset at 151.5°C and a peak at 153.4°C, which is between the melting points of GSF (220.2°C) and 4-*tert*-butylphenol (100.0°C). This observation is consistent with the majority of previously reported cocrystals.[51]

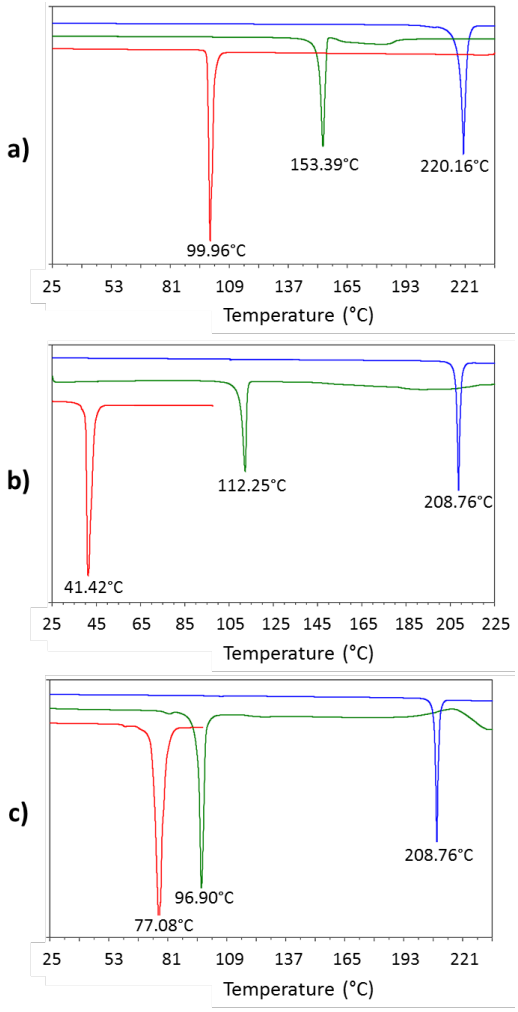

Figure 3. DSC traces of (a) griseofulvin (blue), 4-*tert*-butylphenol (red) and the 1:1 griseofulvin-4-*tert*-butylphenol cocrystal (green); (b) spironolactone (blue), phenol (red) and the 1:1 spironolactone-phenol cocrystal (green); (c) spironolactone (blue), 2,5-xylenol (red) and the 1:1 spironolactone-2,5-xylenol cocrystal (green).

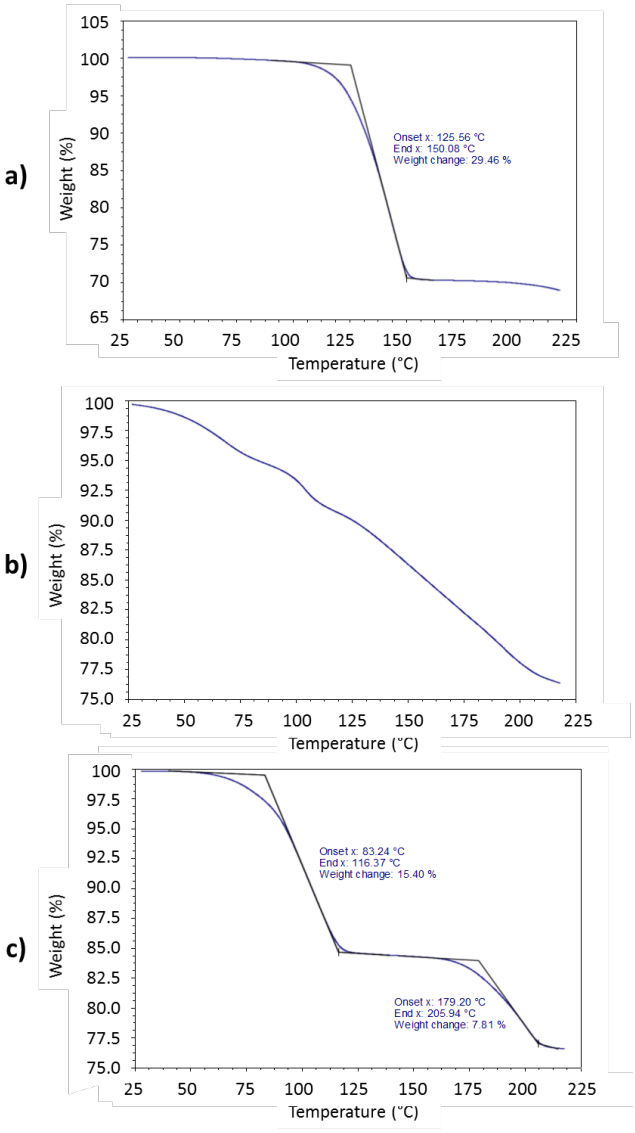

Figure 4. TGA traces of (a) the 1:1 griseofulvin-4-*tert*-butylphenol cocrystal; (b) the 1:1 spironolactone-phenol cocrystal and (c) the 1:1 spironolactone-2,5-xylenol cocrystal.

Weight loss from the cocrystal sample on heating was studied by TGA (Figure 4a). The observed weight loss of 29.5% corresponds to the evaporation or sublimation of 4-*tert*-butylphenol from a 1:1 cocrystal (theoretically 29.8% of the overall molecular weight). There is a single melting endotherm observed during the heating process of the cocrystal at approximately 153°C. It is likely that under the sealed-pan conditions of the DSC experiment, melting of the cocrystal occurs at a lower temperature than the loss of 4-*tert*-butylphenol. In the open-pan TGA experiment, the CCF loss can occur at a temperature below the melting point of the cocrystal. Although the TGA temperature range is considerably lower than the boiling point of 4-*tert*-butylphenol (237°C),[52] sublimation at a lower temperature has been reported previously for cocrystals.[53]

The new phase was analyzed by solid-state infrared spectroscopy (IR). Changes in the IR spectrum are consistent with different intermolecular interactions in the mixed phase compared with the pure components (Figure S4, Appendix). For example, the OH stretch at 3224 cm^{-1} in 4-*tert*-butylphenol is shifted to 3279 cm^{-1} in the new phase.

The crystal structure of the cocrystal was determined from the XRPD pattern. The GSF:4-*tert*-butylphenol cocrystal crystallizes in the monoclinic system with space group $P2_1$ and one molecule of each component in the asymmetric unit. Molecules of GSF interact through C–Cl···O halogen bonds creating chains parallel to the crystallographic 2_1 screw axis (O3···Cl 3.23 Å, O4···Cl 3.22 Å). The main interaction leading to cocrystal formation is a H-bond between the 4-*tert*-butylphenol H-bond donor and the cyclohexenone carbonyl group (Figure 5a).

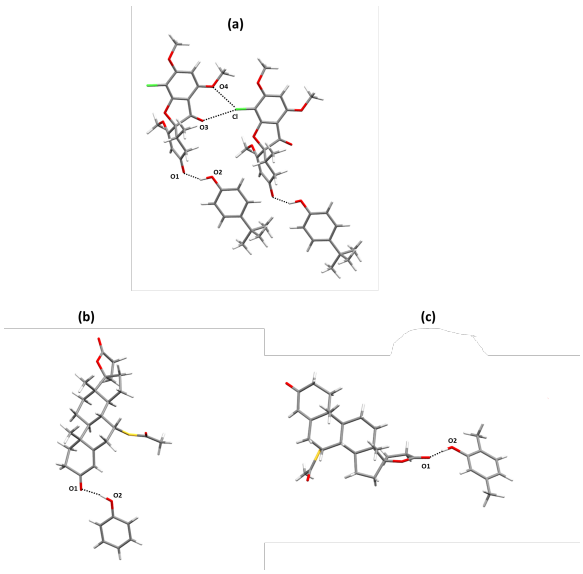

Figure 5. Crystal structures of (a) the 1:1 griseofulvin-4-*tert*-butylphenol cocrystal [d(O1-O2) = 2.545 Å, d(O3-Cl) = 3.231 Å), d(O4-Cl) = 3.216 Å)], (b) the 1:1 spironolactone-phenol cocrystal [d(O1-O2) = 2.767 Å)] and (c) the 1:1 spironolactone-2,5-xylenol cocrystal [d(O1-O2) = 2.891 Å]. The black dotted lines represent H-bonds.

Spironolactone

LAG experiments were initially carried out for 1:1 stoichiometric ratios of SPN to CCFs in the presence of *n*-heptane for 45 minutes at 30 Hz. This led to amorphisation as indicated by a reduction in intensity and sharpness of the X-ray reflections after grinding. To reduce the energy input, the grinding time was reduced to 25 minutes. Novel XRPD patterns were obtained on grinding SPN with CCFs 2,5-dihydroxybenzoic acid, 2,5-xylenol and phenol. The SPN-2,5-dihydroxybenzoic acid XRPD pattern was already reported in a previous study,[38] therefore no further work was carried out on this system. The SPN-2,5-xylenol and SPN-phenol materials obtained were highly crystalline (green traces in Figures 2b and 2c, respectively) and established as phase pure by Pawley fitting of the patterns.

DSC experiments for both new forms showed a sharp, single melting endotherm with a melting point between those of the starting materials, further suggesting cocrystal formation. The

SPN-phenol system has a melting onset at 110.0°C (peak at 112.3°C, Figure 3b green trace), while the SPN-2,5-xylenol material has a melting onset at 95.4°C (peak at 96.9°C, Figure 3c green trace).

TGA of the SPN-phenol cocrystal showed a steady weight loss starting at the beginning of the heating process and still occurring at 225°C. The early change in the sample mass could be caused by the volatile nature of phenol, while further weight loss at high temperatures is most likely due to chemical degradation of the compound. In the TGA trace of the SPN-2,5-xylenol cocrystal, two events were observed: a weight loss of 15.4% between 83.2°C and 116.4°C, followed by another loss of 7.8% between 179.2°C and 205.9°C. The total weight loss of 23.2% can be assigned to the loss of 1 molecule of 2,5-xylenol. There are also obvious differences between the IR spectra of the mixtures and those of the pure solids observed for both of these systems (Figure S5 and S6, Appendix).

Crystal structures of the cocrystals were determined from the XRPD patterns. The SPN-phenol cocrystal has an orthorhombic cell with space group $P2_12_12_1$ and one molecule of each component in the asymmetric unit. The phenol group forms H-bonds as a donor with the cyclohexanone carbonyl group (Figure 5b). The SPN-2,5-xylenol cocrystal has a monoclinic cell with space group $P2_1$ and one molecule of each component in the asymmetric unit. Molecules of SPN interact with 2,5-xylenol molecules through H-bonds between the phenol donor and the furanone acceptor (Figure 5c).

Conclusions

Based on a virtual screening method for cocrystal prediction, an experimental strategy was designed and applied to discover novel cocrystals of two non-ionisable APIs of low aqueous solubility, GSF and SPN. The computational tool compares the stability of a cocrystal to the two components using SSIPs to calculate the difference in the solid state interaction site pairing energies (ΔE). A database of 310 potential CCFs was screened using this approach, and the 35 CCFs that showed the highest values of ΔE were subjected to experimental investigation using liquid-assisted grinding. One GSF cocrystal and two SPN cocrystals were identified, and the crystal structures of the cocrystals were determined from the X-ray powder diffraction patterns. The cocrystals were further analysed by DSC, TGA and IR. Although the identification of three cocrystals after screening 70 CCFs could be seen as a modest success rate, this study demonstrates that computational prediction can be successfully applied to APIs where cocrystal design is difficult due to limited H-bonding potential.

Acknowledgements

We thank AstraZeneca for financial support.

Notes and references

1 S. L. Morissette, Ö. Almarsson, M. L. Peterson, J. F. Remenar, M. J. Read, A. V. Lemmo, S. Ellis, M. J. Cima and C. R. Gardner, *Adv. Drug Delivery Rev.*, 2004**, 56**, 275.

2 C. Leuner and J. Dressman, *Eur. J. Pharm. Biopharm.*, 2000, **50**, 47.

3 J. Alsenz and M. Kansy, *Adv. Drug Delivery Rev.*, 2007, **59**, 546.

4 U. S. Food & Drug, Administration, The Biopharmaceutics Classification System (BCS) Guidance. http://www.fda.gov/AboutFDA/CentersOffices/OfficeofMedicalProductsandTobacco/CDER/ucm128219.htm. (accessed March **2015**)

5 T. Loftsson and D. Duchêne, *Int. J. Pharm.*, 2007, **329**, 1.

6 T. Vasconcelos, B. Sarmento and P. Costa, *Drug Discov. Today*, 2007, **12**, 1068.

7 B. C. Hancock, M. Parks, *Pharm. Res.*, 2000, **17**, 397.

8 J. K. Haleblian, *J. Pharm. Sci.*, 1975, **64**, 1269.

9 Ö. Almarsson, M. J. Zaworotko, *Chem. Commun.*, 2004, 1889.

10 A. D. Bond, *CrystEngComm*, 2007, **9**, 833.

11 (a) http://www.ecfr.gov/cgi-bin/text-idx?c=ecfr&SID=4f70083a7e458a879baeaf15975a0166&rgn=div5&view=text&node=21:3.0.1.1.13&idno=21#21:3.0.1.1.14.2.1.2 (accessed March **2015**); (b) http://www.fda.gov/Food/IngredientsPackagingLabeling/FoodAdditivesIngredients/ucm091048.htm (accessed March **2015**).

12 Everything Added to Food in the United States. http://www.biobased.us/eafus.pdf.

13 (a) A. V. Trask, W. D. Motherwell and W. Jones, *Int. J. Pharm.*, 2006, **320**, 114; (b) D. Good, C. Miranda and N. Rodríguez-Hornedo, *CrystEngComm*, 2011, **13**, 1181.

14 C. C. Sun, *Expert Opin Drug Deliv.*, 2013, **10**, 201.

15 FDA Regulatory Classification of Pharmaceutical Co-crystals 2013. http://www.fda.gov/downloads/Drugs/Guidances/UCM281764.pdf

16 FDA Regulatory Classification of Pharmaceutical Co-crystals Draft Guidance 2016. http://www.fda.gov/ucm/groups/fdagov-public/@fdagov-drugs-gen/documents/document/ucm516813.pdf (accessed November **2016**)

17 P. Stahly, Cocrystals: A Regulatory Rebirth, Whitepaper, Triclinic Labs, 2016.

18 G. P. Stahly, *Cryst. Growth Des.*, 2007, **7**, 1007.

19 P. Vishweshwar, J. A. Mcmahon, J. A. Bis and M. J. Zaworotko, *J. Pharm. Sci.*, 2006, **95**, 499.

20 T. Rager and R. Hilfiker, *Cryst. Growth Des.*, 2010, **10**, 3237.

21 S. J. Nehm, B. Rodríguez-Spong and N. Rodríguez-Hornedo, *Cryst. Growth Des.*, 2006, **6**, 592.

22 T. Friščić and W. Jones, *Cryst. Growth Des.*, 2009, **9**, 1621.

23 (a) S. Karki, L. Fábián, T. Friščić and W. Jones, *Organic Letters*, 2007, **9**, 3133; (b) A. J. Florence, N. Shankland, K. Shankland, W. I. F. David, E. Pidcock, X. Xu, A. Johnston, A. R. Kennedy, P. J. Cox, J. S. O. Evans, G. Steele, S. D. Cosgrove and C. S.Frampton, *J. Appl. Cryst*., 2005, **38**, 249–259.

24 D. Musumeci, C. A. Hunter, R. Prohens, S. Scuderi and J. F. McCabe, *Chem. Sci.*, 2011, **2**, 883.

25 S. Aitipamula, V. R. Vangala, P. S. Chow and R. B. H. Tan, *Cryst. Growth Des.*, 2012, **12**, 5858.

26 K. Yamamoto, S. Tsutsumi and Y. Ikeda, *Int. J. Pharm.*, 2012, **437**, 162.

27 N. Takata, R. Takano, H. Uekusa, Y. Hayashi and K. Terada, *Cryst. Growth Des.*, 2010, **10**, 2116.

28 T. Grecu, C. A. Hunter, E. J. Gardiner and J. F. McCabe, *Cryst. Growth Des.*, 2013, **14**, 165.

29 T. Grecu, H. Adams, C. A. Hunter, J. F. McCabe, A. Portell and R. Prohens, *Cryst. Growth Des.*, 2014, **14**, 1749.
30 (a) C. A. Hunter, *Chem. Sci.*, 2013, **4**, 1687; (b) C. S. Calero, J. Farwer, E. J. Gardiner, C. A. Hunter, M. Mackey, S. Scuderi, S. Thompson and J. G. Vinter, *Phys. Chem. Chem. Phys.,* 2013, **15**, 18262.
31 M. C. Etter, *Acc. Chem. Res.,* 1990, **23**, 120.
32 M. Mukaida, K. Sugano and K. Terada, *Chem. Pharm. Bull.*, 2015, **63**, 18.
33 A. B. Petersen, M. H. Rønnest, T. O. Larsen and M. H. Clausen, *Chem. Rev.*, 2014, **114**, 12088.
34 M. Trotta, M. Gallarate, M. E. Carlotti and S. Morel, *Int. J. Pharm.*, 2003, **254**, 235.
35 M. Wulff and M. Aldén, *Thermochim. Acta*, 1995, **256**, 151.
36 Z. Zili, S. Sfar and H. Fessi, *Int. J. Pharm.*, 2005, **294**, 261.
37 S. Aitipamula, P. S. Chow and R. B. H. Tan, *Acta Crystallogr., Sect. B: Struct. Sci., Cryst. Eng. Mater. **2014**, 70, 54*.
38 Z. Zhong, C. Guo, L. Chen, J. Xu and Y. Huang, *Chem. Commun.*, 2014, **50**, 6375.
39 D. Rathnayake, R. Sinclair, *Skinmed*, 2009, **8**, 328; quiz 333.
40 P. Langguth, A. Hanafy, D. Frenzel, P. Grenier, A. Nhamias, T. Ohlig, G. Vergnault and H. Spahn-Langguth, *Drug. Dev. Ind. Pharm.*, 2005, **31**, 319.
41 J. Chaumeil, *Methods Find. Exp. Clin. Pharmacol.*, 1998, **20**, 211.
42 Cresset torchV10lite http://www.cresset-group.com/products/torchlite/.
43 Gaussian 09, Revision **E.01**, M. J. Frisch, G. W. Trucks, H. B. Schlegel, G. E. Scuseria, M. A. Robb, J. R. Cheeseman, G. Scalmani, V. Barone, B. Mennucci, G. A. Petersson, H. Nakatsuji, M. Caricato, X. Li, H. P. Hratchian, A. F. Izmaylov, J. Bloino, G. Zheng, J. L. Sonnenberg, M. Hada, M. Ehara, K. Toyota, R. Fukuda, J. Hasegawa, M. Ishida, T. Nakajima, Y. Honda, O. Kitao, H. Nakai, T. Vreven, J. A. Montgomery, Jr., J. E. Peralta, F. Ogliaro, M. Bearpark, J. J. Heyd, E. Brothers, K. N. Kudin, V. N. Staroverov, R. Kobayashi, J. Normand, K. Raghavachari, A. Rendell, J. C. Burant, S. S. Iyengar, J. Tomasi, M. Cossi, N. Rega, J. M. Millam, M. Klene, J. E. Knox, J. B. Cross, V. Bakken, C. Adamo, J. Jaramillo, R. Gomperts, R. E. Stratmann, O. Yazyev, A. J. Austin, R. Cammi, C. Pomelli, J. W. Ochterski, R. L. Martin, K. Morokuma, V. G. Zakrzewski, G. A. Voth, P. Salvador, J. J. Dannenberg, S. Dapprich, A. D. Daniels, Ö. Farkas, J. B. Foresman, J. V. Ortiz, J. Cioslowski, and D. J. Fox, Gaussian, Inc., Wallingford CT, 2009.
44 A. Boultif and D. J. Louër, *J. Appl. Cryst.*, 1991, **24**, 987.
45 V. Favre–Nicolin and R. Cerny, *J. Appl. Cryst.*, 2002, **35**, 734.
46 J. Rodriguez–Carvajal, *Physica B.*, 1993, **192**, 55.
47 (a) S. P. Thompson, J. E. Parker, J. Potter, T. P. Hill, A. Birt, T. M. Cobb, F. Yuan and C. C. Tang, *Rev. Sci. Instrum.*, 2009, **80**, 075107; (b) S. P. Thompson, J. E. Parker, J. Marchal, J. Potter, A. Birt, F. Yuan, R. D. Fearn, A. R. Lennie, S. R. Street and C. C. Tang, *J. Synchrotron Radiat.*, 2011, **18**, 637.
48 A. A. Coelho, *TOPAS Academic: General Profile and Structure Analysis Software for Powder Diffraction Data, Version 4.1, Bruker AXS, Karlsruhe, Germany*, 2007.
49 G. S. Pawley, *J. Appl. Cryst.*, 1981, **14**, 357.
50 H. M. Rietveld, *J. Appl. Cryst.*, 1969, **2**, 65.
51 N. Schultheiss and A. Newman, *Cryst. Growth Des.*, 2009, **9**, 2950.
52 M. D. Larrañaga, R. J. Lewis Sr., R. A. Lewis, *Hawley's Condensed Chemical Dictionary*, John Wiley & Sons, Inc. Hoboken, New Jersey, 2016.
53 M. K. Stanton and A. Bak, *Cryst. Growth Des.*, 2008, **8**, 3856.

